Sustainable CO2 adsorbents prepared by coating chitosan onto mesoporous silicas for large-scale carbon capture technology

DOI: 10.1002/ente.201402211

Sustainable CO_2 Adsorbents Prepared by Coating Chitosan onto Mesoporous Silicas for Large-Scale Carbon Capture Technology

Gregor Sneddon,[a] Alexey Y. Ganin,[b] and Humphrey H. P. Yiu*[a]

In this article, we report a new sustainable synthesis procedure for manufacturing chitosan/silica CO_2 adsorbents. Chitosan is a naturally abundant material and contains amine functionality, which is essential for selective CO_2 adsorptions. It is, therefore, ideally suited for manufacturing CO_2 adsorbents on a large scale. By coating chitosan onto high-surface-area mesoporous silica supports, including commercial fumed silica (an economical and accessible reagent) and synthetic SBA-15 and MCF silicas, we have prepared a new family of CO_2 adsorbents, which have been fully characterised with nitrogen adsorption isotherms, thermogravimetric analysis/differential scanning calorimetry, TEM, FTIR spectroscopy and Raman spectroscopy. These adsorbents have achieved a significant CO_2 adsorption capacity of up to 0.98 mmol g^{-1} at ambient conditions ($P=1$ atm and $T=25\,^{\circ}C$). The materials can also be fully regenerated/recycled on demand at temperatures as low as 75 °C with a >85% retention of the adsorption capacity after 4 cycles, which makes them promising candidates for advanced CO_2 capture, storage and utilisation technology.

Introduction

Despite the impressive development of renewable energy sources for power generation, the progress is insufficient for tackling the worldwide problem of increasing "greenhouse gas" emissions from industry, in particular the energy sector.[1] With only a 4% growth predicted for the electricity generated from renewable sources over the next 30 years,[2] CO_2 carbon capture storage (CCS) remains the only viable solution. The world's first commercial CCS plants are already in operation[3] and there has been a strong demand for the development of the current CCS technology to enable the additional step of utilisation of the CO_2. Current CCS technology in the power-generation industry employs amine solutions, such as 30% monoethanolamine in water, for eliminating CO_2 from the flue gas stream.[4] Despite the high recovery rate of CO_2 of up to 98% shown for these solutions,[5] there are numerous disadvantages associated with this technology. These include 1) the high energy consumption required for regenerating the aqueous amine absorbent; 2) degradation of the amine by other flue gas components, for example, SO_2, NO_2, HCl and oxygen; 3) corrosion of equipment; and 4) high toxicity.[6–9] Consequently, new solid-state adsorbents for CO_2 with high specificity and enhanced energy efficiency, handling and regeneration capabilities are needed for fully advancing the carbon capture storage utilisation (CCSU) technology.[10]

Several types of solid adsorbents have been proposed for CCSU, including nanoporous carbon materials, metal organic frameworks, aminated mesoporous silicas and microporous organic polymers.[11–13] With aminated mesoporous silica (NH_2-SBA-15 or NH_2-MCM-41) as an example, this adsorbent shows a good CO_2 capacity adsorption, typically of 1.0–3.6 mmol g^{-1} at $P=1$ atm and $T=25\,^{\circ}C$.[14–16] However, the synthesis of aminated mesoporous silica involves grafting of toxic 3-aminopropyltriethoxysilicate, which is destructive to the mucous membranes and the upper respiratory tract of the human body, and the use of toluene as the solvent in an approximately 100-times quantity (1 g of silica in 100 mL of toluene).[17] For industrial-scale production of adsorbents, the excessive use of aromatic solvents and toxic reagents should be avoided.

Chitosan is a natural polysaccharide that contains randomly distributed D-glucosamine units (see Scheme 1) and has been widely used in various biomedical applications,[18] which indicates its benign nature to humans. Similar to other amine-based adsorbents, CO_2 adsorption can take place on the free amine groups of the D-glucosamine units by the co-operative adsorption of one CO_2 molecule with two adjacent amine groups.[19] Chitosan is a sustainable reagent because it occurs naturally as chitin, which is a major waste product of the seafood industry.[20] Such mass-scale availability presents

[a] G. Sneddon, H. H. P. Yiu
Chemical Engineering, School of Engineering and Physical Sciences
Heriot-Watt University
Edinburgh, EH14 4AS (UK)
E-mail: h.h.yiu@hw.ac.uk

[b] A. Y. Ganin
School of Chemistry
Joseph Black Building
University of Glasgow, Glasgow, G12 8QQ (UK)

Supporting information for this article is available on the WWW under http://dx.doi.org/10.1002/ente.201402211.

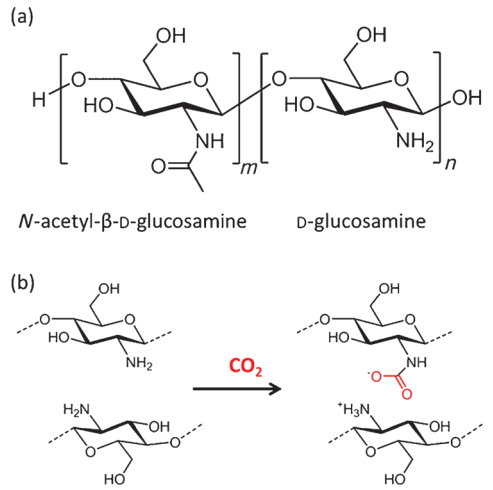

Scheme 1. (a) Structure of chitosan, with the *N*-acetyl-β-D-glucosamine and D-glucosamine units shown. (b) The cooperative adsorption of one CO_2 molecule by two D-glucosamine units of chitosan.

an opportunity to create a viable platform for carbon storage on demand if the problems associated with the low surface area of chitosan and, hence, the low adsorption properties can be resolved. This challenge, however, could be addressed by coating chitosan onto an appropriate support material with a high surface area. For example, Yoshida et al. have coated chitosan onto the macropores of the basic anion-exchange resin HPA 25 and have achieved an adsorption capacity of 0.06 mmol g^{-1} with a chitosan/HPA 25 composite of 27 wt %.[21,22] However, such a low capacity was linked to the surface area of the HPA 25 resin, which is only 23–25 $m^2 g^{-1}$, too low for significant adsorption. To maximise the potential of chitosan as a CO_2 adsorbent, a support material with a much higher surface area will be required.

To address the challenge of finding a highly specific, high-surface-area and low-cost CCSU adsorbent that is capable of releasing CO_2 on demand at low temperatures, we employed a strategy of coating high-surface-area silicas, such as SBA-15 and mesocellular foams (MCFs), with chitosan. Porous silica materials have a good thermal stability and high porosity and have been widely used as industrial adsorbents.[23] This enabled us to develop an efficient, sustainable CO_2 adsorbent, which could lead to a significant advancement towards large-scale production and overcome one major obstacle of CCSU technologies for practical industrial use.

Results and Discussion

Characterisation of silica supports

Fumed silica, a chosen support material for this study, is a commercial mesoporous silica (for example, Cab-O-Sil) with a high surface area (200 $m^2 g^{-1}$) and is widely used in industry,[26] which implies that the chitosan/fumed silica composites developed herein would be suitable for large-scale applications including CO_2 capture. The structural parameters, including the BET surface area, pore size distribution and pore volume, of all silica supports used in this work are summarised in Table 1. The fumed silica support was found to have a BET surface area of 186 $m^2 g^{-1}$ and a pore volume of 0.29 $cm^3 g^{-1}$. Table 1 also shows the structural parameters for two types of synthetic mesoporous silicas (SBA-15 and some MCFs), which were selected for the study of the effect of support's mesoporous structure on the chitosan deposition. The nitrogen adsorption and desorption isotherms for the silica supports shown in Figure 1 b–e exhibit type IV isotherm character with a hysteresis loop, typical for mesoporous materials, whereas fumed silica (Figure 1 a) shows a transitional type II to type IV isotherm as a result of its large mesopores. The pore size distribution of SBA-15 (calculated from the adsorption data; Figure S1 in the Supporting Information) peaks at 8 nm in diameter, which is typical for an SBA-15 sample.

MCFs are essentially pore-expanded SBA-15 with trimethylbenzene (TMB) as the swelling agent. Control of the pore size was achieved by varying the TMB/surfactant ratio; the higher the ratio, the larger the pores were found to be. However, the mesoscale structure becomes less ordered as the TMB/surfactant ratio increases. In contrast to the 2D hexagonal pore array structure of SBA-15, MCF silicas have a "foam-like" (or bubble-like) structure with interconnected cages. In Table 1, the pore volume data is presented as "small" mesopores (<4 nm in diameter), "medium" mesopores (4–10 nm) and "large" mesopores (>10 nm). As a result of the long-range order of tubular pores, the porous structure of SBA-15 is dominated by the medium mesopores (pore volume: 0.7 $cm^3 g^{-1}$). With regard to MCF supports, although the BET surface area decreases as a result of the loss of long-range order, the pore volume of the large mesopores gradually increases from 0.04 $cm^3 g^{-1}$ for SBA-15 to 0.7 $cm^3 g^{-1}$ for MCF-10. Among all MCF samples, the medium mesoporous volume remains roughly unchanged. Such differences in pore volume provide us with a "structural tool" to study the effect of pore size on chitosan deposition and, consequently, CO_2 adsorption capacity.

TEM analysis (Figure 2 a) illustrates the 2D hexagonal mesoporous structure of SBA-15, with a mean pore size of

Table 1. Surface area and pore volume data for all chitosan/mesoporous silicas, as well as fumed silica.

Mesoporous silica support	Unmodified silica					Chitosan on mesoporous silicas				
	BET surface[a] area [$m^2 g^{-1}$]	pore volume [$cm^3 g^{-1}$] total	pore diameter range ≤4 nm	4–10 nm	≥10 nm	BET surface[a] area [$m^2 g^{-1}$]	pore volume [$cm^3 g^{-1}$] total	pore diameter range ≤4 nm	4–10 nm	≥10 nm
fumed silica	186	0.29	0.04	0.07	0.18	123	0.33	0.02	0.05	0.26
SBA-15	530	0.81	0.09	0.70	0.04	376	0.56	0.05	0.49	0.03
MCF-3	439	0.75	0.10	0.20	0.45	187	0.38	0.04	0.11	0.23
MCF-6	387	0.83	0.08	0.18	0.57	210	0.53	0.05	0.11	0.37
MCF-10	375	1.01	0.06	0.25	0.70	241	0.60	0.04	0.16	0.41

[a] Error in samples: ±4 $m^2 g^{-1}$.

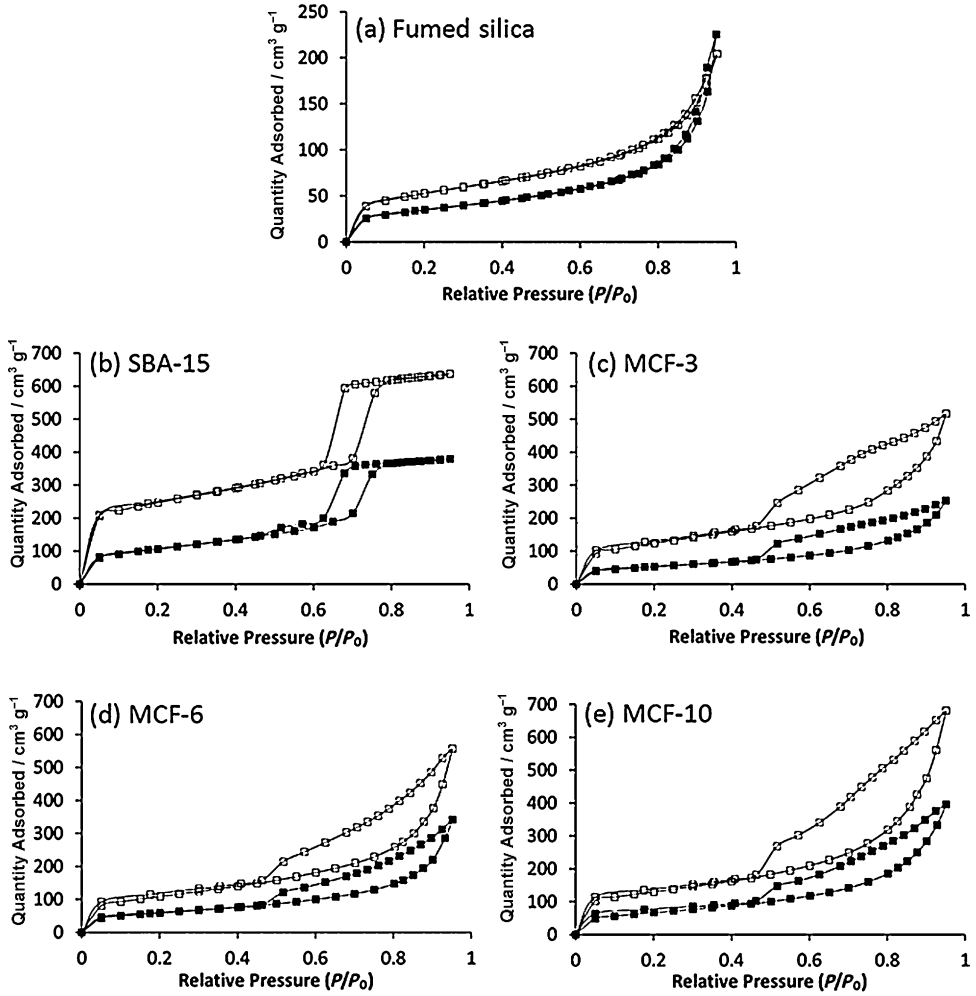

Figure 1. Structural analysis by using N_2 adsorption isotherms for (a) fumed silica, (b) SBA-15, (c) MCF-3, (d) MCF-6 and (e) MCF-10 with (■) and without (□) chitosan. All isotherms show a decrease in the overall N_2 adsorption with incorporation of chitosan. The pore volume decreases with chitosan incorporation because the pores become lined with chitosan or blocked completely.

around 7–9 nm; this is consistent with the pore size distribution data obtained from the N_2 adsorption isotherms. In Figure 2c, the MCF-3 sample shows the effect of the pore expander on the structure of these materials. The hexagonal mesoporous structure of SBA-15 has been completely transformed into a foam-like porous structure. MCF-6 and MCF-10 (Figure 2d and e) showed a similar structure to MCF-3 but the increase in pore size was difficult to depict. The N_2 adsorption isotherm data shown in Table 1 are, therefore, used to confirm the increase in the total pore volume of large mesopores.

Characterisation of chitosan on fumed silica

Initially, chitosan was supported on fumed silica in a range of compositions (7.4, 14, 19, 24, 29 and 32 wt%) to determine the optimal chitosan-to-support ratio. Vibrational spectroscopic analyses (FTIR and Raman spectroscopy) were carried out on chitosan and used as tools to identify the chitosan component on all chitosan/silica samples. The FTIR spectrum for chitosan and the assignment for the peaks are shown in Figure S2 in the Supporting Information. The twin peaks at $\tilde{\nu}=3355$ and 3290 cm^{-1} correspond to the R–NH_2 and R–OH groups. The C–H stretches of the chitosan backbone are shown at $\tilde{\nu}=2910$ and 2870 cm^{-1}. The C=O stretch of the residual *N*-acetyl-β-D-glucosamine units of chitin appears at $\tilde{\nu}=1645$ cm^{-1}, whereas the NH_2 bending vibration appears at $\tilde{\nu}=1590$ cm^{-1}. The C–H bending vibrations are shown at $\tilde{\nu}=1420$, 1375 and 1320 cm^{-1}. The C–O stretches of the alcohol and ether groups can be seen at $\tilde{\nu}=1060$, 1030 and 995 cm^{-1}. FTIR studies were also performed on all of the samples of chitosan deposited on fumed silica (Figure 3a), with the increasing intensity of the peaks corresponding to increasing chitosan content. No peak was observed within the range of 1690–1760 cm^{-1}, which corresponds to carboxylic acid or carboxylate species. Hence, the results suggest that most of the acidic solvent had been removed during drying under vacuum. Also, it is indicated that most of the NH_2 groups on chitosan are not bound to carboxylate ions. Thermogravimetric analysis (TGA) and elemental analysis data were used to verify the composition of each of the samples as accurate (see Table S1 in the Supporting Information).

Raman spectroscopy was used to probe on a microscopic scale the distribution of the chitosan within the sample. It is, therefore, a complementary technique to the FTIR spectroscopy, which is a bulk technique and probes the presence of chitosan in the sample without giving a distinct answer about the distribution of the chitosan in the silica matrix. Whereas the control sample of pristine fumed silica did not show any significant Raman activity, even a small amount of chitosan (7.4 wt%) was sufficient for observing the characteristic signals of the chitosan molecule, as indicated in the Figure 3b. In contrast, the same sample showed very low peak intensity on its FTIR spectrum (Figure 3a). Furthermore, the intensity of the Raman signals also increases with the amount of the chitosan present in the sample. The most distinct peaks in the spectra are at $\tilde{\nu}=2900/2933$ and 3311 cm^{-1} and are associated with the R_2–CH_2 and R–NH_2 groups stretching fre-

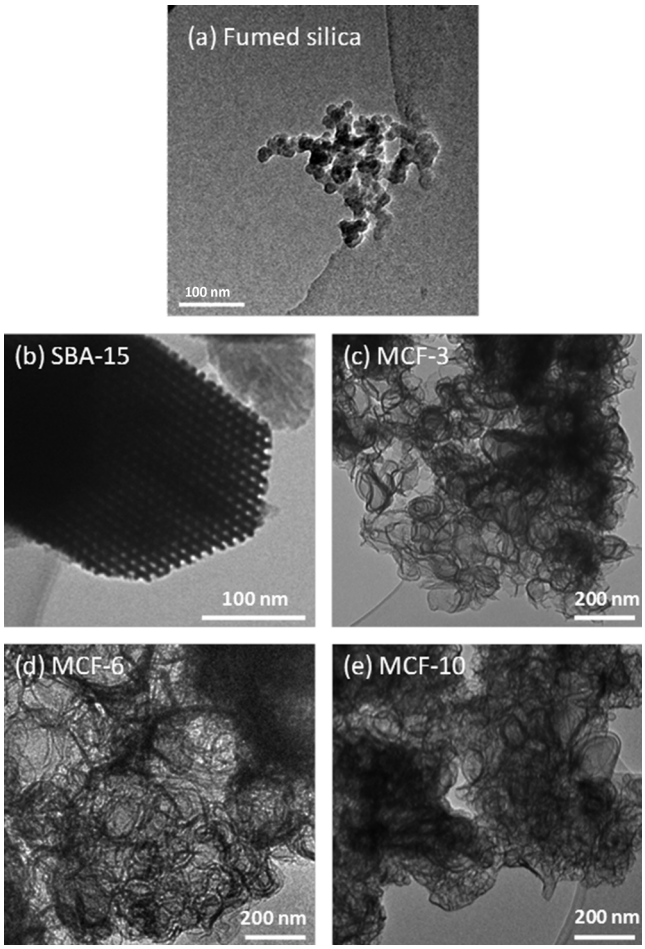

Figure 2. TEM micrographs of (a) fumed silica, (b) SBA-15, (c) MCF-3, (d) MCF-6, and (e) MCF-10. SBA-15 shows a highly ordered hexagonal porous array with a *p6mm* symmetry, whereas the MCF samples show foam-like structures.

quencies.[25] The clear split of the R_2–CH_2 group signal is a result of out-of-phase and in-phase bond stretching vibrations. Indeed, characterisation with Raman spectroscopy instead of FTIR spectroscopy avoids the interference from the silica support, a distinct advantage for characterising samples with a low organic content. Figure 3c shows the Raman map of a 19 wt% chitosan/fumed silica particle and the chitosan is shown to be evenly distributed at a μm scale. Chitosan has a large amount of hydroxy groups, so it is likely that the chitosan interacts with the silica support through strong hydrogen bonds between these OH groups and the Si–OH groups on the silica surface.

From the analysis with N_2 adsorption isotherms, pure chitosan has been shown to have a very low BET surface area (0.31 $m^2 g^{-1}$) and a pore volume of 0.0016 $cm^3 g^{-1}$, which suggests that it is virtually non-porous; these results lead to a negligible CO_2 adsorption capacity, consistent with the findings of Yoshida et al.[21] This illustrates the need for the deposition of chitosan on a suitable support and for maximising the CO_2 adsorption capacity of a natural amine material. The thermal stability of chitosan was studied by simultaneous TGA/differential scanning calorimetry (DSC) analysis (Figure 4a). There is an initial endothermic weight loss at approximately $T = 100\,^{\circ}C$, which corresponds to removal of water from the sample. Thermal decomposition, associated with a large exothermic peak, starts at about $T = 230\,^{\circ}C$, which indicates that chitosan can be used at an elevated temperature range. There is no recordable change (for example, glass transition) for chitosan between $T = 100$–$200\,^{\circ}C$.

From the N_2 adsorption isotherm analysis, there was a gradual decrease in the BET surface area as the chitosan content of the composite samples increased (Table 2). The chitosan

Table 2. Surface area values for chitosan deposited on a fumed silica support.

Chitosan content [wt%] on fumed silica (1 g)	Mass of chitosan added in synthesis [g]	Measured BET surface area[a] [$m^2 g^{-1}$]
0	0	186
0 (control)[b]	0	188
7.4	0.08	153
14	0.16	136
19	0.24	123
24	0.32	109
29	0.40	80
32	0.48	65

[a] Error in BET surface area: ± 3 $m^2 g^{-1}$. [b] Fumed silica sample treated with acetic acid.

can fill up the mesopores of the fumed silica support, so the available surface area decreases. If the pore volume data of the chitosan/silica composites was examined in detail according to the small (<4 nm), medium (4–10 nm) and large (>10 nm) mesopore classification (see Table 1), the chitosan/fumed silica samples showed a decrease in both the small (pore volume changes from 0.04 to 0.02 $cm^3 g^{-1}$) and medium (pore volume changes from 0.07 to 0.05 $cm^3 g^{-1}$) mesopore regions as a result of pore blockage. Interestingly, the pore volume of the large mesopore range (>10 nm) increased from 0.18 to 0.26 $cm^3 g^{-1}$ after coating with chitosan. This may be caused by large pores created from interconnecting the fumed silica particles with chitosan. Overall, this leads to an increase in the total pore volume upon deposition of chitosan from 0.29 to 0.33 $cm^3 g^{-1}$. This phenomenon becomes more transparent from Figure S3 in the Supporting Information, in which the pore size distributions of samples with various chitosan contents are presented. Upon incorporation of 7.4 wt% chitosan into the pore network of fumed silica, there was a decrease in the pore volume with pore sizes below 8 nm relative to the results with the fumed silica support. However, an increase in the pore volume was observed at pore sizes of >10 nm. Notably, pure, unsupported chitosan is non-porous with a low BET surface area and pore volume (0.13 $m^2 g^{-1}$ and 0.0016 $m^3 g^{-1}$, respectively) and the coating process is unlikely to break up the porous structure of fumed silica to form new larger pores of >10 nm. Hence, the assumption of large pores created by interconnecting fumed silica particles offers a reasonable explanation for this observation. For samples with a higher percentage of chitosan (>

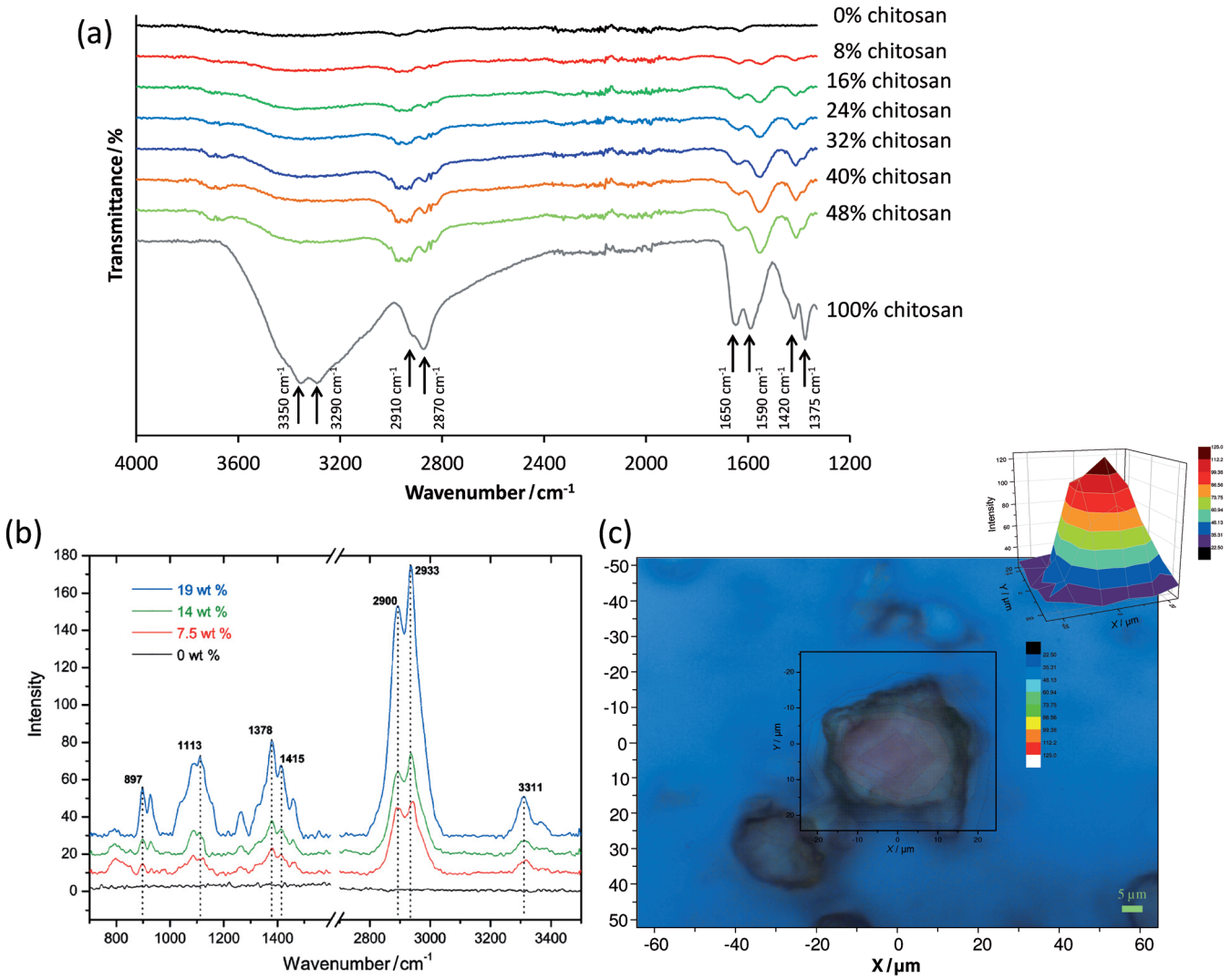

Figure 3. (a) FTIR spectra of chitosan and fumed silica composites with increasing chitosan content. (b) Raman spectra of pure fumed silica (0 wt%) and chitosan-containing composites with increasing chitosan content. (c) Raman mapping of a chitosan/fumed silica composite, which shows even distribution of chitosan throughout the pores of the fumed silica.

24 wt%), the surface areas and pore volumes of the samples decrease significantly and are likely to reduce the CO_2 adsorption capacity. The 19 wt% chitosan sample still retains a high surface area (123 $m^2 g^{-1}$) and pore volume (0.33 $cm^3 g^{-1}$), yet has a significant chitosan loading. Therefore, 19 wt% chitosan was chosen as a benchmark loading for this work.

Characterisation of chitosan on mesoporous silicas

Chitosan (19 wt%) was coated on SBA-15 (chitosan/SBA-15), MCF-3 (chitosan/MCF-3), MCF-6 (chitosan/MCF-6) and MCF-10 (chitosan/MCF-10) in order to study the effect of the porosity of the support on the chitosan deposition and on the CO_2 adsorption capacity. These composite materials showed no significant difference in the FTIR analysis in comparison to pure chitosan, with all samples showing peaks associated with both chitosan and silica (Figure S2b in the Supporting Information). The organic content from TGA analysis of the composite materials was found to be consistent across all chitosan/mesoporous silica samples (see TGA data in Figure S4 and Table S1 in the Supporting Information). The surface area and pore size distribution data in Table 1 show a decrease of 30–50% in the pore volume in both the medium (4–10 nm) and large mesopore ranges (>10 nm), which suggests that chitosan has been coated evenly across all pore ranges. Hence, there was no apparent preference for deposition/blockage to one particular pore range, which would have led to an overall decrease in the total pore volume and the BET surface area. If the chitosan was only deposited on the exterior of the support without entering the mesopores, such a high amount (19 wt%) would have led to a large decrease in both pore volume and BET surface area. Our results suggested that chitosan entered the pores, aided by sonication during deposition. These samples retained a high BET surface area (187–376 $m^2 g^{-1}$), which was adequate for use as gas adsorbents.

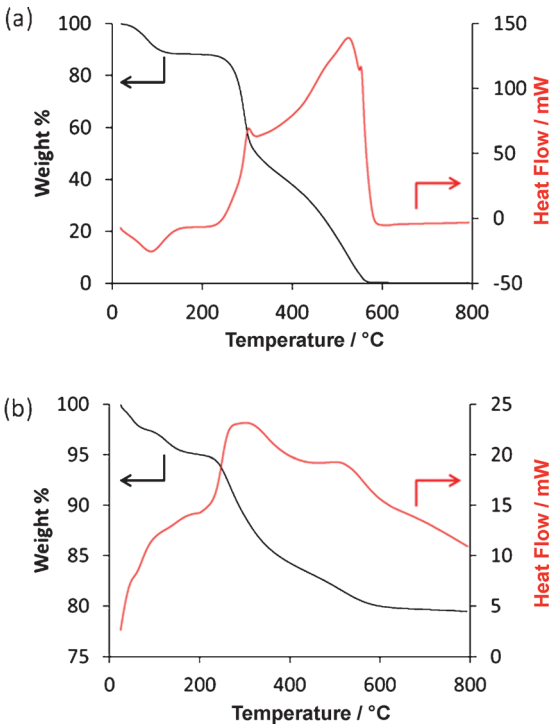

Figure 4. (a) TGA/DSC traces of pure chitosan from $T = 20$–$800\,^{\circ}C$ with air as the carrier gas to show thermal decomposition of the chitosan. Thermal decomposition begins at approximately $T \approx 200\,^{\circ}C$. (b) TGA/DSC traces for the 19 wt% chitosan/fumed silica sample with air as the carrier gas. Thermal decomposition starts at $T \approx 200\,^{\circ}C$, which is similar to the pure chitosan sample in (a).

Volumetric and gravimetric CO_2 adsorption analysis

The CO_2 capacity of the chitosan/silica composites was measured with two different methods: volumetric and gravimetric adsorptions. The volumetric CO_2 adsorption capacity of the 19 wt% chitosan/fumed silica sample was found to be 0.29 mmol g^{-1} and that measured gravimetrically was 0.09 mmol g^{-1} (Table 3). No uptake of CO_2 was recorded from the gravimetric measurement for a pure fumed silica sample (see Figure S5 in the Supporting Information), which indicates that the CO_2 uptake from these samples is attributed to the coated chitosan. With consideration that pure chitosan has a CO_2 adsorption capacity of approximately 0.02 mmol g^{-1},[21] our results show a remarkable 23-fold increase in capacity per unit mass of chitosan (0.47 mmol $g^{-1}_{chitosan}$), a unique property of these chitosan/silica composites. The higher capacity measured from the volumetric analysis than from the gravimetric measurement is consistent with other works in the literature.[26] The difference between these two measuring systems is that the gravimetric analysis was carried out in a dynamic flow system, whereas a static closed system was used for the volumetric measurement. Moreover, a 50% CO_2 in N_2 purge stream was used for the gravimetric measurements, instead of 100% CO_2 for the latter. In the next section, we will discuss the effect of CO_2 concentration in the gas adsorbate on the CO_2 adsorption capacity.

Table 3. Volumetric and gravimetric CO_2 adsorption capacities measured for chitosan/mesoporous silica adsorbents.

CO_2 adsorbent	Volumetric capacity (100% CO_2) [mmol g^{-1}]	Gravimetric capacity (50% CO_2 in N_2) [mmol g^{-1}]
chitosan/fumed silica (19 wt%)	0.29	0.09
chitosan/SBA-15	0.80	0.32
chitosan/MCF-3	0.98	0.34
chitosan/MCF-6	0.75	0.29
chitosan/MCF-10	0.79	0.26

The results of the volumetric CO_2 adsorption analysis for the chitosan on mesoporous silica supports (SBA-15 and MCFs) are shown in Figure 5 and Table 3. The chitosan/

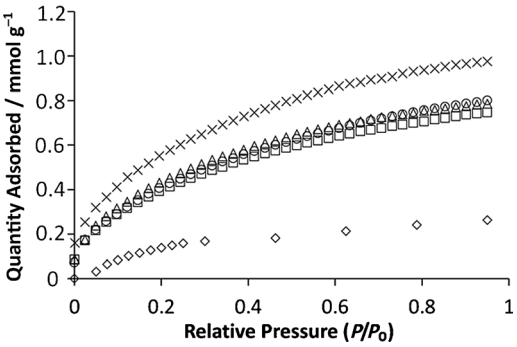

Figure 5. Volumetric CO_2 adsorption isotherms of chitosan/fumed silica (◇), chitosan/SBA-15 (○), chitosan/MCF-3 (×), chitosan/MCF-6 (□) and chitosan/MCF-10 (△). The CO_2 adsorption capacity recorded is in the order: chitosan/MCF-3 > chitosan/SBA-15 > chitosan/MCF-10 > chitosan/MCF-6 > chitosan/fumed silica.

MCF-3 sample has the highest adsorption capacity at 0.98 mmol g^{-1}, whereas other samples vary from 0.75–0.80 mmol g^{-1}. These recorded capacities are comparable with other high-surface-area nanomaterials designed for CO_2 adsorption, such as metal organic frameworks (for example, MOF-5 with a capacity of approximately 2 mmol g^{-1}, measured with a volumetric method).[27] Indeed, we can compare this result in terms of adsorption efficiency (that is, CO_2/NH_2 ratio) with an adsorbent of similar structure, NH_2-MCM-41, which gives a CO_2 adsorption capacity of 1.0 mmol g^{-1} at $P = 1$ atm and $T = 20\,^{\circ}C$.[15] NH_2-MCM-41 has a concentration of 2.48 mmol g^{-1} of NH_2 groups, which results in a CO_2/NH_2 ratio of 0.4. The chitosan/MCF-3 sample has a concentration of approximately 0.76 mmol g^{-1} of NH_2 groups (based on the elemental analysis) and a CO_2/NH_2 ratio of 1.3, which can be viewed as a 3-fold increase in efficiency compared with that of NH_2-MCM-41. In theory, the adsorbent with the highest BET surface area should adsorb the highest amount of CO_2 as a result of physisorption. However, this was not observed in this case because chitosan/MCF-3 had the lowest BET surface area among all of the samples except chitosan/fumed silica (Table 1). There is also no clear correlation between the pore volume of the adsorbents and their CO_2 adsorption

capacity (Table 1 and 3), which suggests a complex relationship between adsorption and the structural parameters (surface area and pore volume). Notably, these structural parameters were measured for the whole composite, with no distinction between the gas adsorption (N_2 or CO_2) from the silica surface or from the chitosan coating. It would be difficult to pinpoint the critical structural factor influencing the overall CO_2 adsorption capacity.

Similar to that for chitosan/fumed silica, the adsorption results from the gravimetric analysis show a lower capacity for all chitosan on mesoporous silica samples relative to the adsorption capacity from the volumetric method (Table 3). Nonetheless, the CO_2 adsorption capacity of all chitosan/silica composite samples follows the same trend; the gravimetric adsorption is approximately one third of the volumetric adsorption capacity. On comparison between these two techniques, the CO_2 adsorption capacity measured with the gravimetric method is more representative of the real adsorption from a flowing flue gas, in contrast to the volumetric measurement from a closed system. Therefore, many recent research works in the literature have adopted the gravimetric method for measuring the CO_2 adsorption capacity for adsorbents.[28–30]

Gas composition analysis

In order to examine the effect of the CO_2 content in a gas stream on the adsorption capacity, gravimetric analysis with four CO_2 in N_2 gas compositions (100, 50, 13 and 8%) was also carried out with chitosan/MCF-3, which had shown the highest capacity, as the adsorbent (Figure S6 in the Supporting Information). With a 100% CO_2 stream, a maximum adsorption capacity of 0.42 mmol g^{-1} was achieved quickly, within $T=30$ min, which was faster than with a 50% CO_2 stream ($T=90$ min). Gas streams containing 13 and 8% CO_2 were used to simulate the CO_2 content in the flue gas from coal-fired and gas-fired power stations, respectively. In both cases, the same adsorption capacity (0.10 mmol g^{-1}) was recorded after $T=90$ min. This suggested that chitosan/MCF-3 has the potential to be used as a CO_2 adsorbent for power stations, with a reasonable capacity achieved by utilising a waste polymer material as the major component for adsorption.

Water is another flue gas component (around 6–15%) to influence the efficiency of CO_2 adsorbents during carbon capture. Many solid-state adsorbents, such as zeolites and metal organic frameworks, can be deactivated by high moisture content. On the other hand, aminated silicas have not shown deactivation and, in some instances (for example, SBA-15 grafted with ethylenediamine groups), have shown an improved CO_2 adsorption capacity and adsorption efficiency in presence of water.[16] The chitosan/silica composites also utilise surface amine groups for interaction with CO_2; hence, deactivation by water is unlikely. Indeed, these composites were prepared in an aqueous medium and so water should have little negative effect on their adsorption behaviour.

Regeneration study

In addition to the adsorption capacities, the study of the regeneration of the materials at a low temperature is also important. A high energy requirement for regenerating the liquid amine absorbent (for example, 10–30% monoethanolamine in water is regenerated at $T=140$ °C) in conventional carbon capture systems presents a major obstacle for a wider application. During the regeneration of these liquid-phase systems, much of the energy was spent on the evaporation of water, which is the "non-adsorptive" component of the adsorbent. To circumvent this obstacle, water-free solid-state adsorbents with a low regeneration temperature ($T<100$ °C) are preferred.

In our regeneration study, four adsorption–regeneration cycles were carried out with the chitosan/MCF-3 sample, as shown in Figure 6. The overall adsorption for each cycle retained a minimum of 88% of the capacity from the previous cycle and the overall drop in capacity is less than 15% over 4 cycles. Therefore, this adsorbent can be regenerated at a low temperature ($T=75$ °C) with little loss in adsorption capacity. A higher retention of capacity, up to 98%, can be achieved by regeneration at $T=100$ °C but this would lead to higher energy consumption. In comparison with solid state CaO adsorbent, which has been suggested for large-scale carbon capture but requires a high-temperature regeneration at $T=700$ °C,[31] our chitosan/MCF-3 adsorbent represents a significant advancement in terms of reducing the energy consumption for regeneration, saving operational costs and, more importantly, reducing the overall carbon footprint. One interesting feature in this study was that there was a "stepwise" weight loss after every regeneration cycle without effect on the adsorption. This may be as a result of the displacement of strongly bound water or acetic acid from the adsorbent by adsorbed CO_2. During regeneration, these molecules (water and acetic acid) left the system as the CO_2 was

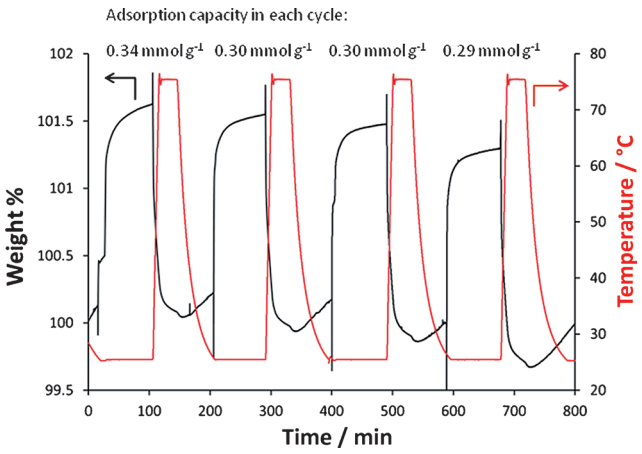

Figure 6. Gravimetric adsorption of CO_2 by chitosan/MCF-3. Four regeneration cycles are shown with a $t=90$ min adsorption at $T=25$ °C and a $t=30$ min desorption at $T=75$ °C. The adsorption capacity measured for each cycle is shown above the corresponding adsorption peak.

desorbed at $T=75\,^{\circ}C$. Nonetheless, this feature has no impact on the overall performance of the adsorbent.

Conclusions

A family of chitosan/mesoporous silica composite materials were prepared with a simple deposition method. Unlike many other solid-state adsorbents, including aminated mesoporous silicas, metal organic frameworks and carbon nanotubes, the procedure for preparing these materials follows closely the green chemistry principles (room temperature and pressure conditions, avoidance of the use of toxic solvents, with 0.2 M acetic acid as the only solvent, and minimum waste emissions). These adsorbents, with a maximum volumetric CO_2 adsorption capacity of 0.98 mmol g^{-1} at $T=25\,^{\circ}C$, are also chemically and thermally stable (up to $T=200\,^{\circ}C$). More importantly, they can be regenerated at a low temperature of $T=75\,^{\circ}C$ and retained 85% capacity after 4 cycles. Such low energy consumption is advantageous for industrial applications, particularly in comparison with liquid-phase monoethanolamine solutions, which require an energy-intensive regeneration regime.

Chitosan is a major food waste product and to make use of it for tackling another environmental problem is an attractive approach. Large-scale use of the chitosan/fumed silica composite can be easily adapted because both chitosan and fumed silica are already commonly used in industries. To further enhance the CO_2 adsorption capacity, mesoporous silicas with high surface areas (for example, SBA-15 and MCF-3) can be used as the support material. These mesoporous silicas synthesised from surfactant templates have yet to be widely used in industry but room-temperature synthesis methods and continuous preparation processes have already been reported.[32] Surfactant-free preparation routes have also been reported in the literature.[33] Therefore, large-scale use of these high-surface-area silicas could be possible in the near future. Alternatively, if there is a new non-silica material with a high surface area and a similar porous structure to MCF-3, coating chitosan onto it could give similar adsorptive properties to those chitosan/MCF-3.

Currently, the high running cost associated with carbon capture technology is one major obstacle for carbon capture storage (CCS) to become popular and the energy required for adsorbent regeneration contributes significantly to this cost. To fully realise the potential of carbon capture technologies, a lowering of the running costs is fundamental. The low-cost sustainable preparation of adsorbents in a large quantity, together with the low-temperature regeneration, presented herein can reduce the overall operational cost for CCS. Furthermore, green CO_2 adsorbents, such as the chitosan/mesoporous silica composites from this work, will have to be considered in order to achieve a net reduction of the carbon footprint.

Experimental Section

Materials

Low-molecular-weight chitosan (75–85% deacetylated), fumed silica with a BET surface area of approximately 200 $m^2 g^{-1}$ (data provided by supplier), glacial acetic acid (99.7%), tetraethyl orthosilicate (TEOS, 98%) and 1,3,5-trimethylbenzene (TMB or mesitylene, 98%) were all purchased from Sigma–Aldrich. Concentrated hydrochloric acid (37%) was supplied by Fisher Scientific. Pluronic P123 surfactant ($EO_{20}PO_{70}EO_{20}$, EO: ethylene oxide, PO: propylene oxide, $M_w=5800$) was kindly donated by BASF. Deionised water was used in all experimental procedures. All chemicals were used as received without further purification. All gases used (N_2, He, and CO_2, all >99.99%,) were supplied by BOC.

Synthesis and characterisations for SBA-15 and MCF mesoporous silicas

The procedure for preparing SBA-15 was selected because of its high reproducibility.[34] In a typical synthesis, Pluronic P123 surfactant (4 g) was first dissolved in an acidic solution containing concentrated hydrochloric acid (10 mL) and deionised water (139 mL) at $T=30\,^{\circ}C$. After the surfactant was fully dissolved, TEOS (8.3 g) was added dropwise and the reaction mixture was allowed to stir for $t=24$ h at $T=30\,^{\circ}C$. The solution was then transferred to a polytetrafluoroethylene bottle and heated in an oven to $T=100\,^{\circ}C$ for $t=72$ h. The white precipitates were then filtered off with a Büchner flask and funnel and allowed to dry overnight. The white solid was then calcined in air at $T=550\,^{\circ}C$ for $t=6$ h to remove the surfactant template.

For MCF support materials, the same procedure as that for the SBA-15 synthesis was carried out but the pore-expanding agent TMB (1.2, 2.4 and 4.0 g) was added to the surfactant solution and allowed to dissolve completely prior to the addition of TEOS.[35] The samples were also calcined at $T=550\,^{\circ}C$ for $t=6$ h. These materials were denoted as MCF-*n*, in which *n* indicates the TMB/P123 weight-to-weight ratio; hence, MCF-3 has a TMB/P123 ratio of 0.3 (that is, 1.2 g of TMB and 4.0 g of P123).

Coating chitosan on silica supports

To determine the optimum chitosan/silica ratio, a series of samples were prepared with fumed silica as a model support material. In a typical experiment, the fumed silica support (1.0 g) was mixed with a chitosan solution (0.08, 0.16, 0.24, 0.32, 0.40 and 0.48 g of chitosan to give 7.4, 14, 19, 24, 29 and 32 wt% samples, respectively) in acetic acid (20 mL, 0.2 M). Once mixed, the fumed silica/chitosan solutions were sonicated in an ultrasonic bath for 1 h to degas the samples and encourage pore filling with the chitosan solution. After degassing, the sample suspensions were transferred to petri dishes to dry at room temperature in a fume cupboard. Petri dishes were used to increase the evaporation rate of the acetic acid. After 48 h of drying, the samples were then dried in a vacuum oven at $T=50\,^{\circ}C$ and with a reduced pressure of $P\approx20$ mbar overnight to remove residual acetic acid. The dried samples were finally ground with a mortar and pestle. The supported chitosans are notated as chitosan/support with the designated chitosan content in wt%. For example, chitosan/fumed silica (19 wt%) refers to 19 wt% of chitosan on fumed silica, which was prepared with 0.24 g of chitosan and 1 g of sup-

port. Chitosan supported on other mesoporous silica samples (19 wt%) were similarly prepared by using silica support (1 g; SBA-15, MCF-3, MCF-6 or MCF-10) with a chitosan solution containing chitosan (0.24 g, based on the results from chitosan/fumed silica samples) and acetic acid (20 mL, 0.2 M).

Sample characterisation

The structural characters of SBA-15 and the MCFs were studied with nitrogen adsorption–desorption isotherms and TEM. The N_2 adsorption–desorption isotherms were measured with a Micromeritics Gemini VII 2390p unit. All samples were outgassed at $T=80\,^{\circ}C$ under flowing nitrogen for $t=2$ h by using a Flowprep unit (Micromeritics). Nitrogen adsorption–desorption isotherms were recorded at $T=-196\,^{\circ}C$. The BET surface area, pore size distribution and Barrett–Joyner–Halenda pore volume were calculated by using Micromeritics software V1.03A. TEM analysis was carried out with a Tecnai T20 microscope (200 keV).

The chitosan/mesoporous silica samples were characterised with nitrogen adsorption isotherms, TGA, elemental analysis and vibration spectroscopies (FTIR and Raman). BET surface area and pore volume analysis was carried out with a Micromeritics Gemini VII 2390P unit with the same procedure as that described above. Thermal analysis (simultaneous TGA and DSC) was performed with a TA Instruments SDT Q600 thermobalance. TGA and DSC data were collected between $T=20$ and $800\,^{\circ}C$ at a heating rate of $10\,^{\circ}C\,min^{-1}$ with air as the carrier gas. Elemental analysis was carried out with a CE 440 elemental analyser. Carbon, hydrogen and nitrogen contents (as percentages) in samples were determined to an error of $\pm 0.15\%$. The FTIR spectra were recorded with a Perkin–Elmer Spectrum 100 spectrophotometer. Spectra were collected in the wavenumber range between $\tilde{\nu}=650$–$4000\,cm^{-1}$ with 16 scans at a resolution of $4\,cm^{-1}$. Raman spectroscopy was carried out on a powdered sample on a Horriba LabRam-HR spectrometer operated in back-scattered geometry with a 532 nm laser at ambient temperature over a sample area of $100\,\mu m^2$. Calibration was performed by referencing the spectrometer to the $520.1\,cm^{-1}$ silicon line. The typical acquisition times were 6×30 s. Several spectra recorded at different points for each probed sample indicated consistently that the peaks were associated with the spectra of chitosan. The Raman imaging technique was also employed over a wider area of $50\times60\,\mu m$ on a selected sample to probe the bulk character of the coated materials and to test the distribution of the chitosan within the composite materials.

Volumetric and gravimetric CO_2 uptake and regeneration study by using adsorption isotherms and TGA

The volumetric adsorption study ($P/P_0=0$–760 mm Hg) was carried out by using a Micromeritics Gemini VII 2390p unit fitted with a chiller bath set at $T=25\,^{\circ}C$. The samples were outgassed at $T=80\,^{\circ}C$ under flowing N_2 prior to CO_2 adsorption measurement. For the gravimetric adsorption measurements, the SDT Q600 unit was used with a cyclic custom programme. Samples were activated at $T=75\,^{\circ}C$ overnight prior to adsorption studies. After activation, the samples were cooled down to $T=25\,^{\circ}C$ and a 50:50 gaseous mixture of CO_2:N_2 was purged through the sample for 90 min once the weight stabilised. After 90 min of exposure, the temperature was raised to $T=75\,^{\circ}C$ at a rate of $5\,^{\circ}C\,min^{-1}$ and held at $T=75\,^{\circ}C$ for a further 30 min to allow CO_2 desorption and, hence, regeneration of the samples to be complete. The temperature was then decreased to $T=25\,^{\circ}C$ for the second adsorption loop. This procedure was repeated for four cycles to test the regeneration of the chitosan/MCF-3 sample. CO_2 adsorption tests were also carried out at varying CO_2:N_2 volume ratios (100, 13 and 8% CO_2) with the chitosan/MCF-3 sample. These experiments were carried out to mimic the flue gas environment of coal-fired (13% CO_2) and gas-fired (8% CO_2) power stations.

Acknowledgements

The authors acknowledge financial support from the EPSRC S&I Award (EP/F034482/1), the EPSRC AMPGas consortium (EP/J02077X/1) and the Scottish Carbon Capture and Storage (SCCS) programme. We also acknowledge the Kelvin Nanocharacterisation Centre, University of Glasgow, for their assistance in TEM imaging.

Keywords: adsorption · carbohydrates · carbon storage · mesoporous materials · silicates

[1] L. Li, N. Zhao, W. Wei, Y. Sun, *Fuel* **2013**, *108*, 112.
[2] U.S. Energy Information Administration (EIA), *Annual Energy Outlook 2014 (AEO2014) Early Release Overview*, **2013**, http://www.eia.gov/forecasts/aeo/er/pdf/0383er(2014).pdf, accessed on 03 December 2014.
[3] R. Trager, *Chem. World* **2014**, *11*, 8.
[4] B. A. Oyenekan, G. T. Rochelle, *AIChE J.* **2007**, *53*, 3144.
[5] A. Yamasaki, *J. Chem. Eng. Jpn.* **2003**, *36*, 361.
[6] M. S. Ojala, N. F. Serrano, P. Uusi-Kyyny, V. Alopaeus, *Fluid Phase Equilib.* **2014**, *376*, 85.
[7] D. J. Fauth, E. A. Frommell, J. S. Hoffman, R. P. Reasbeck, H. W. Pennline, *Fuel Process. Technol.* **2005**, *86*, 1503.
[8] K. P. Resnik, J. T. Yeh, H. W. Pennline, *Int. J. Environ. Technol. Manage.* **2004**, *4*, 89.
[9] J. T. Yeh, K. P. Resnik, K. Rygle, H. W. Pennline, *Fuel Process. Technol.* **2005**, *86*, 1533.
[10] L. Espinal, D. L. Poster, W. Wong-Ng, A. J. Allen, M. L. Green, *Environ. Sci. Technol.* **2013**, *47*, 11960.
[11] G. Sneddon, A. Greenaway, H. H. P. Yiu, *Adv. Energy Mater.* **2014**, *4*, 1301873.
[12] D. M. D'Alessandro, B. Smit, J. R. Long, *Angew. Chem. Int. Ed.* **2010**, *49*, 6058; *Angew. Chem.* **2010**, *122*, 6194.
[13] S. Choi, J. H. Drese, C. W. Jones, *ChemSusChem* **2009**, *2*, 796.
[14] H. Y. Huang, R. T. Yang, D. Chinn, C. L. Munson, *Ind. Eng. Chem. Res.* **2003**, *42*, 2427.
[15] M. R. Mello, D. Phanon, G. Q. Silveira, P. L. Llewellyn, C. M. Ronconi, *Microporous Mesoporous Mater.* **2011**, *143*, 174.
[16] F. Y. Chang, K. J. Chao, H. H. Cheng, C. S. Tan, *Sep. Purif. Technol.* **2009**, *70*, 87.
[17] L. X. Zhang, C. C. Yu, W. R. Zhao, Z. L. Hua, H. R. Chen, L. Li, J. L. Shi, *J. Non-Cryst. Solids* **2007**, *353*, 4055.
[18] J. Berger, M. Reist, J. M. Mayer, O. Felt, N. A. Peppas, R. Gurny, *Eur. J. Pharm. Biopharm.* **2004**, *57*, 19.
[19] A. Danon, P. C. Stair, E. Weitz, *J. Phys. Chem. C* **2011**, *115*, 11540.
[20] M. Rinaudo, *Prog. Polym. Sci.* **2006**, *31*, 603.
[21] H. Yoshida, S. Oehlenschlaeger, Y. Minami, M. Terashima, *J. Chem. Eng. Jpn.* **2002**, *35*, 32.
[22] H. Yoshida, S. Oehlenschlaeger, Y. Minami, M. Terashima in *Proceedings of the Second Pacific Basin Conference on Adsorption Science and Technology* (Ed.: D. D. Do), World Scientific, Singapore, **2000**, pp. 693–697.
[23] X. Li, B. H. Li, J. J. Deng, T. T. Lu, S. Wang, J. B. Li, D. S. Chen, Y. Q. Liu, S. H. Wang, *Ind. Eng. Chem. Res.* **2014**, *53*, 11137.

[24] "Silica": O. W. Flörke, H. A. Graetsch, F. Brunk, L. Benda, S. Paschen, H. E. Bergna, W. O. Roberts, W. A. Welsh, C. Libanati, M. Ettlinger, D. Kerner, M. Maier, W. Meon, R. Schmoll, H. Gies, D. Schiffmann in *Ullmann's Encyclopedia of Industrial Chemistry, Vol. 32*, Wiley-VCH, Weinheim, **2008**, pp. 421–508.
[25] N. B. Colthup, L. H. Daly, S. E. Wiberley, *Introduction to Infrared and Raman Spectroscopy*, 3rd ed., Academic, London, **1990**, pp. 387–481.
[26] R. Babarao, J. Jiang, *Langmuir* **2008**, *24*, 6270.
[27] Z. Zhao, X. Ma, A. Kasik, Z. Li, Y. S. Lin, *Ind. Eng. Chem. Res.* **2013**, *52*, 1102.
[28] X. Wang, C. Song, A. M. Gaffney, R. Song, *Catal. Today* **2014**, *238*, 95.
[29] Y. Labreche, Y. Fan, F. Rezaei, R. P. Lively, C. W. Jones, W. J. Koros, *ACS Appl. Mater. Interfaces* **2014**, *6*, 19336.
[30] Y. Han, G. Hwang, H. Kim, B. Z. Haznedaroglu, B. Lee, *Chem. Eng. J.* **2015**, *259*, 653.
[31] S. P. Wang, L. J. Fan, C. Li, Y. J. Zhao, X. B. Ma, *ACS Appl. Mater. Interfaces* **2014**, *6*, 18072.
[32] J. Jammaer, T. S. van Erp, A. Aerts, C. E. A. Kirschhock, J. A. Martens, *J. Am. Chem. Soc.* **2011**, *133*, 13737.
[33] S. C. Kung, C. C. Chang, W. Fan, M. A. Snyder, *Langmuir* **2014**, *30*, 11802.
[34] H. H. P. Yiu, M. A. Keane, Z. A. D. Lethbridge, M. R. Lees, A. J. El Haj, J. Dobson, *Nanotechnology* **2008**, *19*, 255606.
[35] P. Schmidt-Winkel, C. J. Glinka, G. D. Stucky, *Langmuir* **2000**, *16*, 356.

Received: December 16, 2014
Revised: January 21, 2015
Published online on ■■ ■■, 0000

